J Biomol NMR (2013) 56:303–311
DOI 10.1007/s10858-013-9767-1

COMMUNICATION

Efficient band-selective homonuclear CO–CA cross-polarization in protonated proteins

Veniamin Chevelkov · Chaowei Shi · Hannes Klaus Fasshuber · Stefan Becker · Adam Lange

Received: 4 June 2013 / Accepted: 30 July 2013 / Published online: 8 August 2013

Abstract Previously introduced for highly deuterated proteins, band-selective magnetization transfer between CO and CA spins by dipolar-based homonuclear cross polarization is applied here to a protonated protein. Robust and efficient recoupling is achieved when the sum of effective radio-frequency fields on CO and CA resonances equals two times the spinning rate, yielding up to 33 % of magnetization transfer efficiency in protonated ubiquitin. The approach is designed for moderate magic-angle spinning rates and high external magnetic fields when the isotropic chemical shift difference of CO and CA considerably exceeds the spinning rate. This method has been implemented in $N_iCO_{i-1}CA_{i-1}$ and $CA_i(N_i)CO_{i-1}CA_{i-1}$ two-dimensional interresidual correlation experiments for fast and efficient resonance assignment of ubiquitin by solid-state NMR spectroscopy.

Keywords Solid-state magic-angle spinning NMR · Homonuclear recoupling · Protein resonance assignment · Microcrystalline ubiquitin

Electronic supplementary material The online version of this article (doi:10.1007/s10858-013-9767-1) contains supplementary material, which is available to authorized users.

V. Chevelkov · C. Shi · H. K. Fasshuber · S. Becker · A. Lange (✉)
Max Planck Institute for Biophysical Chemistry, Göttingen, Germany
e-mail: adla@nmr.mpibpc.mpg.de

C. Shi
School of Life Sciences, University of Science and Technology of China, Hefei, China

Introduction

Solid-state magic-angle spinning (MAS) NMR has made significant progress in the determination of protein structure (Wasmer et al. 2008; McDermott 2009; Jehle et al. 2010; Bayro et al. 2011; Huber et al. 2011; Loquet et al. 2012; Sengupta et al. 2012; Asami et al. 2013; Hong and Schmidt-Rohr 2013; Weingarth and Baldus 2013) and dynamics (Chevelkov et al. 2009; Schanda et al. 2010; Lewandowski 2013). This became possible in part due to recent hardware developments resulting in higher external magnetic fields and faster MAS rates.

Nowadays, spectrometers with external magnetic fields corresponding to proton Larmor frequencies between 800 and 1,000 MHz are becoming more and more available for the study of complex biomolecules. At higher external fields, higher MAS rates are preferable for efficient CSA suppression to minimize spinning sidebands thus simplifying and increasing the intensity of multidimensional spectra. Changes in the experimental conditions very often require modifications of existing and development of new protocols for the best experimental performance.

A crucial step for site-specific protein characterization is the resonance assignment. For carbon-detected solid-state NMR on uniformly [^{13}C, ^{15}N]-labeled proteins the most commonly applied approach is based on two- and three-dimensional (2D and 3D) versions of hetero- and homonuclear correlation experiments such as NCO, NCA, NCOCX, NCACX, CA–CA and CX–CX (Pauli et al. 2001; Igumenova et al. 2004; Shi et al. 2009; Schuetz et al. 2010). One essential component in these pulse schemes is the CO–CA magnetization transfer needed to obtain interresidual correlations between N of a given residue and CA of the previous residue. A number of recoupling techniques can be employed for this step, the most common being proton-driven spin diffusion

(PDSD) (Szeverenyi et al. 1982), DARR/RAD (Takegoshi et al. 2001; Morcombe et al. 2004), DREAM (Verel et al. 2001), HORROR (Nielsen et al. 1994), rotational resonance recoupling in the tilted rotating frame (R2TR) (Takegoshi et al. 1995), RFDR (Bennett et al. 1998) and MIRROR (Scholz et al. 2008), where the choice is mostly determined by the experimental conditions. A detailed overview of modern recoupling methods can be found elsewhere (De Paepe 2012; Mithu et al. 2013). At an external magnetic field corresponding to 850 MHz proton Larmor frequency and a spinning rate of 20 kHz the above listed recoupling methods could be not optimal for CO–CA polarization exchange: PDSD and DARR/RAD suffer from an increased Zeeman energy difference and homonuclear coupling suppression, DREAM and HORROR are not applicable since the isotropic chemical shift difference of CO and CA considerably exceeds the spinning rate, R2TR is a too narrow-banded scheme. RFDR proved to be a very simple and efficient approach to transfer magnetization from CA to CO spins with up to ~35 % magnetization transfer efficiency at moderate MAS rates (~10 kHz) in a perdeuterated protein (Huang et al. 2011) and in a protonated AGG sample, employing high-power proton decoupling (Bayro et al. 2009). At high external magnetic fields, RFDR requires higher ^{13}C RF field strength for broader excitation band width and thus extremely high proton power for heteronuclear decoupling (Bennett et al. 1998; Bayro et al. 2008), which is not feasible in applications to sensitive biomolecules. Recent studies have shown that RFDR can also be efficient even without high-power proton decoupling (Bayro et al. 2008) at fast MAS rates around 30 kHz, but exact transfer rates were not reported. So far, the performance of RFDR without high-power heteronuclear decoupling at the MAS rate of 20 kHz—as employed in our study—has not been studied yet, to the best of our knowledge. MIRROR is a band-selective second-order recoupling technique and at the considered conditions also too narrow banded. Additionally, the reported maximal efficiency of polarization transfer (Scholz et al. 2008) for two carbon resonances in a model compound is lower than the efficiency we could achieve in a protein with band-selective recoupling (vide infra).

In this communication we show that the previously introduced band-selective homonuclear CP (BSH-CP) scheme (Chevelkov et al. 2013) for efficient magnetization transfer between CO and CA spins in deuterated proteins can be used in protonated proteins as well. The approach is designed for moderate magic-angle spinning rates (ca. 20 kHz) and high external magnetic fields (corresponding to 700–900 MHz of proton resonance frequency) where the isotropic chemical shift difference of CO and CA considerably exceeds the spinning rate. Both zero- and double-quantum homonuclear recoupling can be achieved by continuous RF irradiation, if the Hartmann–Hahn condition is satisfied, i.e. if the sum or difference of the effective fields acting on CO and CA is equal to one or two times the spinning rate. One potential draw-back of BSH-CP is related to comparatively long recoupling times, as discussed in detail before (Chevelkov et al. 2013). In case of deuterated samples where no high-power proton decoupling needs to be applied this is not a severe limitation. However, these long recoupling times may prohibit the application to protonated proteins due to the requirement of high-power proton-carbon decoupling. We show here that efficient recoupling can be obtained at moderately long recoupling times around 4–5 ms and moderately high recoupling powers around 70 kHz, enabling very useful applications of BSH-CP to protonated proteins. The most efficient recoupling is achieved when the sum of effective radio-frequency fields equals two times the spinning rate, yielding a transfer efficiency of up to 33 %. Here we applied this method to obtain $N_iCO_{i-1}CA_{i-1}$ and $CA_i(N_i)CO_{i-1}CA_{i-1}$ 2D correlation spectra of protonated, uniformly [^{13}C, ^{15}N]-labeled ubiquitin. Supplemented by 2D C–C PDSD and NCA spectra these data allow for a rapid, and almost complete, backbone resonance assignment.

Materials and methods

Sample preparation

Uniformly [^{13}C, ^{15}N]-labeled ubiquitin was prepared as described earlier (Lazar et al. 1997). Approximately 20 mg of material, precipitated using poly(ethylene glycol) (PEG) (Seidel et al. 2005), was transferred into a 3.2 mm rotor.

Solid state NMR spectroscopy

All experiments were conducted on a 20 T wide-bore spectrometer (Bruker Biospin, Germany) equipped with an Avance III console and a (^{1}H, ^{13}C, ^{15}N) triple-resonance 3.2 mm probe. The employed MAS rates were 21 and 11 kHz. The effective sample temperature was 8 ± 2 °C as measured by the temperature-dependent water proton resonance relative to an internal DSS reference (Boeckmann et al. 2009). At 21 kHz MAS, we tested the efficiency of BSH-CP with a 1D version of a BSH-CP based NCOCA experiment, in comparison to results from 1D versions of standard PDSD-based NCOCX as well as NCO, NCA and ^{13}C-CP experiments. To assess the efficiency of this method for resonance assignment we recorded at this spinning rate also several 2D correlation spectra based on BSH-CP: $N_iCO_{i-1}CA_{i-1}$ (BSH-CP-NCOCA) and $CA_i(N_i)CO_{i-1}CA_{i-1}$, as well as standard NCA and ^{13}C–^{13}C PDSD spectra. For comparison, 2D NCOCX correlation spectra employing PDSD for CO–CA

magnetization transfer were obtained at spinning frequencies of 21 and 11 kHz.

The pulse sequences for the 2D BSH-CP-NCOCA and $CA_i(N_i)CO_{i-1}CA_{i-1}$ experiments are shown in Fig. 1a, b, respectively. All other experiments used routine protocols which can be found elsewhere (Baldus et al. 1998; Pauli et al. 2001). The BSH-CP-NCOCA spectrum was recorded in 12.5 h using 128 scans, a 3.2 s interscan delay, and maximum isotropic chemical shift evolution times of 13.5 and 9.5 ms for ^{15}N and ^{13}C, respectively. Similar parameters were employed for the $CA_i(N)COCA_{i-1}$ correlation spectrum: The overall measurement time was 36.5 h, with 384 scans, an interscan delay of 3.3 s, and maximum isotropic chemical shift evolution times in the indirect and direct dimensions of 8 and 9 ms, respectively. The experiment is conceptually similar to the CA_i–CA_{i-1} correlation experiment previously described by Siemer et al., (2006) but benefits from the improved efficiency of CO–CA polarization transfer due to the application of BSH-CP (Chevelkov et al. 2013) instead of R2TR (Takegoshi et al. 1995).

In Fig. 1, open, filled and hacked bars represent hard 180°, 90° and trim pulses. Typical radiofrequency (RF) strength of proton and carbon hard pulses was set to 83 and 49 kHz, respectively. During direct and indirect isotropic chemical shift evolution periods of ^{13}C and ^{15}N nuclei, SPINAL-64 (Fung et al. 2000) heteronuclear decoupling was applied on the ^{1}H channel with an RF strength of 78 kHz. WALTZ-64 (Shaka et al. 1983) decoupling with an RF field strength of 2.5 kHz was applied on the ^{15}N channel during ^{13}C evolution and detection periods to remove heteronuclear scalar couplings. A hard 180° pulse was applied on the ^{13}C channel to remove scalar couplings during ^{15}N indirect evolution periods. 78, 76 and 71 kHz CW decoupling were applied on the ^{1}H channel during CA–N, N–CO SPECIFIC CP (Baldus et al. 1998) and BSH-CP transfer steps, respectively. CO–CA BSH-CP was achieved by applying a continuous RF irradiation during 4 ms in the middle of the CA band with an average RF strength of 13.2 kHz and a linear ramp from 100 to 80 %. Prior to BSH-CP, the CO magnetization was flipped by a 63° hard trim pulse along the effective BSH-CP RF field. After BSH-CP, a second 50 kHz hard trim pulse was applied during 4.4 μs on-resonance with CA to bring the CO magnetization to the X axis without affecting the CA magnetization. The phases of both trim pulses with respect to the BSH-CP spin lock pulse are depicted in Fig. 1a, b. SPECIFIC CP (Baldus et al. 1998) was used for N–CO polarization transfer by applying a constant RF field of 8.8 kHz on ^{13}C and on ^{15}N an RF field with initial strength of 13.5 kHz ramped down linearly to 80 %. In BSH-CP-NCOCA and $CA_i(N)COCA_{i-1}$ experiments, contact times for the NCO CP step of 3 and 3.6 ms, respectively, were used. For the CA–N SPECIFIC CP step we used a constant ^{15}N RF field of 5 kHz, while the RF field on CA was ramped down to 80 % from an initial value of 17.1 kHz. The contact time was 3.5 ms.

Initial ^{1}H–^{15}N and ^{1}H–^{13}CA magnetization transfer was achieved by CP with contact times of 340 and 190 μs, respectively. The ^{1}H RF field strength was ramped down to 80 % with an average value of 53 kHz, while the RF field on the X channel was 53 kHz minus the spinning frequency to satisfy the n = 1 Hartmann-Hahn condition.

An NCA correlation spectrum (Baldus et al. 1998) was recorded at a spinning rate of 21 kHz within 3.3 h with 32 scans, a 3.5 s interscan delay, and maximum acquisition times of 13 and 10 ms for ^{15}N and ^{13}C isotropic chemical shift evolution, respectively. A ^{13}C–^{13}C correlation experiment with a PDSD mixing time of 50 ms was recorded in 19.2 h with 40 scans, a 2.7 s interscan delay, and maximum ^{13}C isotropic chemical shift evolution times in the indirect and direct dimensions of 11 and 15 ms, respectively.

For comparison with BSH-CP-NCOCA, two NCOCX experiments were recorded at MAS rates of 21 and 11 kHz, using a PDSD mixing time of 50 ms for CO-CX transfer. At the MAS rate of 21 kHz we used 64 scans, a 3.5 s interscan delay, and maximum evolution times of 10 ms in both dimensions. The total experimental time was 4.3 h. At the MAS rate of 11 kHz we used 192 scans, a 3 s interscan delay, and 11 and 10 ms for maximum ^{15}N and ^{13}C isotropic chemical shift evolution times, respectively. The total experimental time was 14.5 h. The applied RF fields

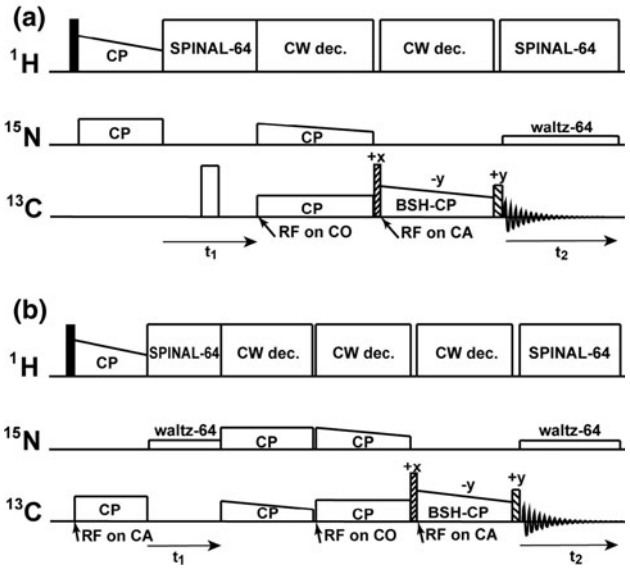

Fig. 1 The general pulse sequence for **a** 2D NCOCA and **b** 2D $CA_i(N)COCA_{i-1}$ correlation experiments based on band-selective homonuclear (BSH) CP transfer from CO to CA under continuous RF irradiation when the Hartmann-Hahn condition is satisfied

were similar to the ones used for BSH-CP-NCOCA and $CA_i(N)COCA_{i-1}$ experiments.

Results and discussion

A detailed quantum–mechanical description of two dipolar-coupled homonuclear spins in a powdered solid under MAS and continuous RF irradiation has been presented earlier (Nielsen et al. 1994; Takegoshi et al. 1995). Recoupling takes place at various conditions when the modulations of the spatial and spin parts of the spin Hamiltonian mutually cancel each other. At the given experimental conditions, recoupling of the flip–flop and flop–flop terms that correspond to n = 1, ZQ and n = 2, DQ transitions, respectively, occurs when the difference or sum of the effective fields acting on CO and CA is equal to one (n = 1, ZQ) or two (n = 2, DQ) times the spinning rate, respectively (Chevelkov et al. 2013). At an external magnetic field of 20 T (850 MHz ^{1}H Larmor frequency) and at 21 kHz MAS, the n = 1, ZQ and n = 2, DQ recoupling conditions for CO (resonance at 178 ppm) and CA (resonance at 58 ppm) spins are therefore fulfilled at carbon RF field strengths equal to 5.2 and 13.1 kHz, respectively, applied on resonance on CA. In our previous studies of band-selective homonuclear (BSH) CP (Chevelkov et al. 2013), we considered in detail a number of relevant parameters determining the performance of this technique, which is based on continuous RF irradiation. Recoupling scaling factors, magnetization transfer dynamics, optimal irradiation frequency, robustness with respect to RF field miscalibration and inhomogeneity as well as isotropic chemical shift variations were analyzed analytically and/or numerically. The experimental results revealed very high magnetization transfer rates of up to 50 % from CO to CA in a deuterated protein. A potential problem in the application of the scheme to protonated proteins lies in the heat deposition associated with heteronuclear decoupling during BSH-CP, which ultimately limits the maximum length of the recoupling period and thus the transfer efficiency.

Figure 2 shows the CO–CA homonuclear magnetization transfer efficiency as a function of the applied RF field strength on CA (top panel) and as a function of the BSH-CP contact time (middle panel) for the n = 2, DQ recoupling condition and as a function of the applied ^{1}H CW decoupling RF field strength (bottom panel) for the n = 2, DQ recoupling condition. One-dimensional experiments were performed according to the pulse scheme shown in Fig. 1a, with the ^{13}C field ramped down to 80 % during BSH-CP. The top panel reveals magnetization transfer at both recoupling conditions, namely n = 1, ZQ and n = 2, DQ at maximum RF field strengths of ca. 5.9 and 14.6 kHz, respectively. Due to the amplitude variation from 100 to 80 %, the fields of 5.9 and 14.6 kHz need to be multiplied by a factor of 0.9 yielding 5.3 and 13.1 kHz as the average values, in excellent agreement with the theoretical expectations. The first trim pulse (see Fig. 1a) was set to 63° during the whole optimization. For the top panel we used a contact time of 4.5 ms and 71 kHz of ^{1}H CW decoupling power. For the middle panel we used 14.6 kHz of maximum ^{13}C RF field strength and 71 kHz of ^{1}H CW decoupling power. For the bottom panel we set the CO–CA contact time to 6.75 ms and the ^{13}C RF recoupling field to 14.6 kHz. The optimization reveals that DQ transfer provides higher transfer efficiency compared to ZQ transfer, as described earlier (Chevelkov et al. 2013). The magnetization builds up relatively slowly and reaches a maximum after 5 ms for the n = 2, DQ recoupling condition, as plotted in the middle panel. Finally, the bottom panel shows the dependence of magnetization transfer efficiency on the employed ^{1}H CW decoupling RF field. The maximum transfer rate was 33 % at a contact time of 6.75 ms and with a ^{1}H decoupling field of 98.5 kHz, as determined by comparing integral values of initial CO band and final CA band signals. The proton decoupling power can be set to 71 kHz as a good compromise between performance on

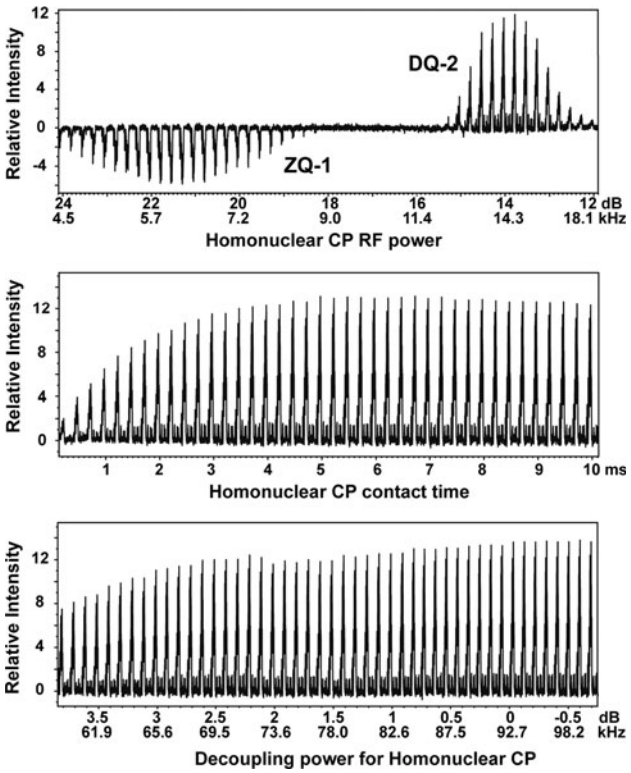

Fig. 2 CA magnetization signal after CO-CA BSH-CP transfer as a function of maximal RF field strength applied on CA (*top*), BSH-CP contact time (*middle*), and decoupling power on protons (*bottom*). All spectra were acquired on a 20 T wide-bore spectrometer at an MAS frequency of 21 kHz. The data in the *middle* and *bottom panels* were recorded for the n = 2, DQ recoupling condition

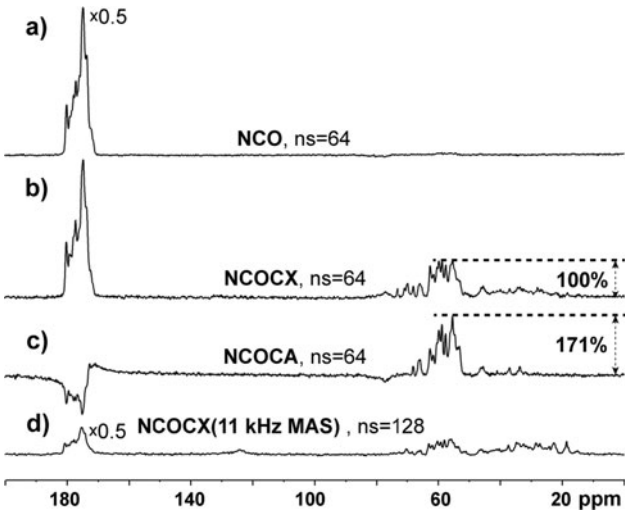

Fig. 3 **a** NCO, **b** PDSD-based NCOCX, and **c** BSH-CP based NCOCA 1D spectra of uniformly [^{13}C, ^{15}N]-labeled ubiquitin at 21 kHz MAS, as well as **d** a PDSD-based NCOCX spectrum recorded at 11 kHz MAS. All spectra at 21 kHz MAS (**a**–**c**) were recorded with 64 scans, whereas the spectrum at 11 kHz MAS (**d**) was recorded with 128 scans. The spectra in **a** and **d** are scaled down by a factor of 2

one hand and sample and hardware safety on the other hand.

We compared the performance of BSH-CP at an MAS rate of 21 kHz with the performance of PDSD in NCOCX experiments at MAS rates of 21 and 11 kHz. We employed PDSD as an illustrative reference for its clarity, easy and error-free set up and the fact that this experiment is well known and widely used for assignment, despite the fact that it does not deliver highest performance. Figure 3 shows ^{13}C spectra obtained with 1D versions of NCO, NCOCX, and BSH-CP NCOCA experiments recorded at an MAS rate of 21 kHz with 64 scans and an NCOCX 1D ^{13}C spectrum recorded at 11 kHz MAS with 128 scans. For the BSH-CP step in the NCOCA experiment the contact time was set to 4.5 ms and the proton CW decoupling power during recoupling to 71 kHz. A PDSD time of 100 ms was employed in both NCOCX spectra. The NCO spectrum and the NCOCX spectrum obtained at 11 kHz have been scaled down by a factor of 2 in Fig. 3a, d. The integrated CA band signal after BSH-CP in the NCOCA experiment is 30 % from the integrated initial CO band signal detected in the NCO experiment. At the same time, the CA signal intensity in the BSH-CP NCOCA spectrum is around 10 and 30 % of the CA signal intensity in standard HCA and NCA cross polarization experiments. The high performance of the recoupling scheme may be further improved up to 33 % by using longer contact times and/or higher proton decoupling power, as indicated in Fig. 2. Table 1 summarizes the observed CO–CA transfer rates in PDSD-based experiments compared to the performance of BSH-CP recoupling. The BSH-CP based scheme provides around 1.6 times higher magnetization transfer efficiency compared to the NCOCX scheme based on PDSD with 100 ms mixing time at 21 kHz MAS, as obtained by integrating the CA bands. The amplitude of the CA signal in the BSH-CP-NCOCA spectrum is 1.7 times higher than in the PDSD-based NCOCX spectrum (171 %, see panels b and c). Because PDSD is known to become inefficient at high MAS rates we also recorded an NCOCX spectrum at 11 kHz MAS. However, we find that at 11 kHz MAS, the efficiency of polarization transfer to CA after PDSD with 100 ms mixing time is 1.2 times less compared to the experiment recorded at 21 kHz MAS. This can be explained in part by the observation, that spin diffusion to side chains is quenched at higher MAS, while at 11 kHz MAS it is very efficient, resulting in reduced CA signal. Surprisingly, the CO–CA transfer during PDSD at an MAS rate of 21 kHz was relatively efficient, while the spin diffusion from CA to side chains was almost quenched. This may be explained by near rotational resonance conditions (Raleigh et al. 1988; Seidel et al. 2004) for CA–CO spin pairs, even though the average chemical shift difference for a CA–CO spin pair is $\sim$25.5 kHz and considerably exceeds the spinning frequency. Importantly, we found that despite careful optimizations, SPECIFIC CP NCO transfer at 11 kHz was twice less efficient compared to NCO transfer at 21 kHz. Usually in PDSD-based NCOCX

Table 1 Selected experimental parameters and CO–CA transfer efficiencies obtained in 1D PDSD-based NCOCX spectra

Experiment type	Number of scans	MAS rate, kHz	CO–CA transfer efficiency in PDSD-based experiments[a]		
			Relative to BSH-CP recoupling, mixing time		
			100 ms	50 ms	20 ms
NCO	64	21			
NCOCA	64	21			
NCOCX	64	21	1/1.6 = 0.63	1/(1.6·1.2) = 0.52	1/(1.6·1.6) = 0.39
NCOCX	128	11	1/(1.6·1.2) = 0.52	1/(1.6·1.2·1.1) = 0.47	1/(1.6·1.2·1.1) = 0.47

[a] The transfer efficiency is given relative to the transfer efficiency obtained in the BSH-CP NCOCA experiment by comparing integrals of the CA band

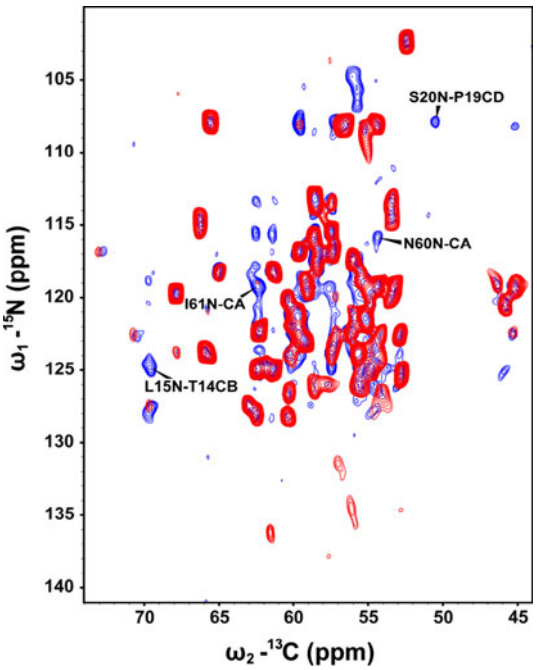

Fig. 4 Overlay of 2D BSH-CP-NCOCA (*red*) and 2D NCOCX (*blue*) spectra of uniformly [^{13}C, ^{15}N]-labeled ubiquitin. The NCOCA spectrum was acquired at an MAS frequency of 21 kHz with a 4 ms BSH-CP contact time, within a total experimental time of 12.5 h. The NCOCX spectrum was acquired at an MAS frequency of 11 kHz with PDSD transfer for 50 ms within 14.5 h of total experimental time. Prior to Fourier-transformation, the data of both spectra were apodized in both dimensions with a 51°-shifted squared sine bell window function

experiments shorter mixing times are employed to prevent inter-residual CO–CA or CA–CA transfer during the PDSD mixing step. Mixing times between 20 and 50 ms are suitable for exclusively intra-residual magnetization transfer. At an MAS rate of 21 kHz, the CA signal intensity obtained with mixing times of 20 and 50 ms (data not shown) was 1.6 and 1.2 times less compared to the CA signal intensity recorded with a mixing time of 100 ms. The transfer dynamics are different at 11 kHz MAS: The CA signal intensity obtained with mixing times of 20 and 50 ms was 1.1 times less in both cases (data not shown) compared to the CA signal intensity recorded with a mixing time of 100 ms.

Two-dimensional NCOCX spectra recorded at MAS rates of 11 and 21 kHz with a PDSD mixing time of 50 ms show a sizeable number of cross peaks, which are not interresidual correlations between N_i and CA_{i-1} nuclei. Thus, significantly shorter PDSD times are required for exclusive one bond CO–CA transfer. In contrast, BSH-CP NCOCA spectra exhibit exclusively N_i–CA_{i-1} correlations, because different from the second-order PDSD phenomenon, BSH-CP employs a first-order recoupling effect and the undesired sequential CO–CA and CA–CA transfers are suppressed by dipolar truncation (Hodgkinson and Emsley 1999; Bayro et al. 2009). Figure 4 compares a 2D BSH-CP-NCOCA spectrum recorded at 21 kHz MAS with 4 ms recoupling with a 2D NCOCX spectrum recorded at 11 kHz MAS with a mixing time of 50 ms. The above

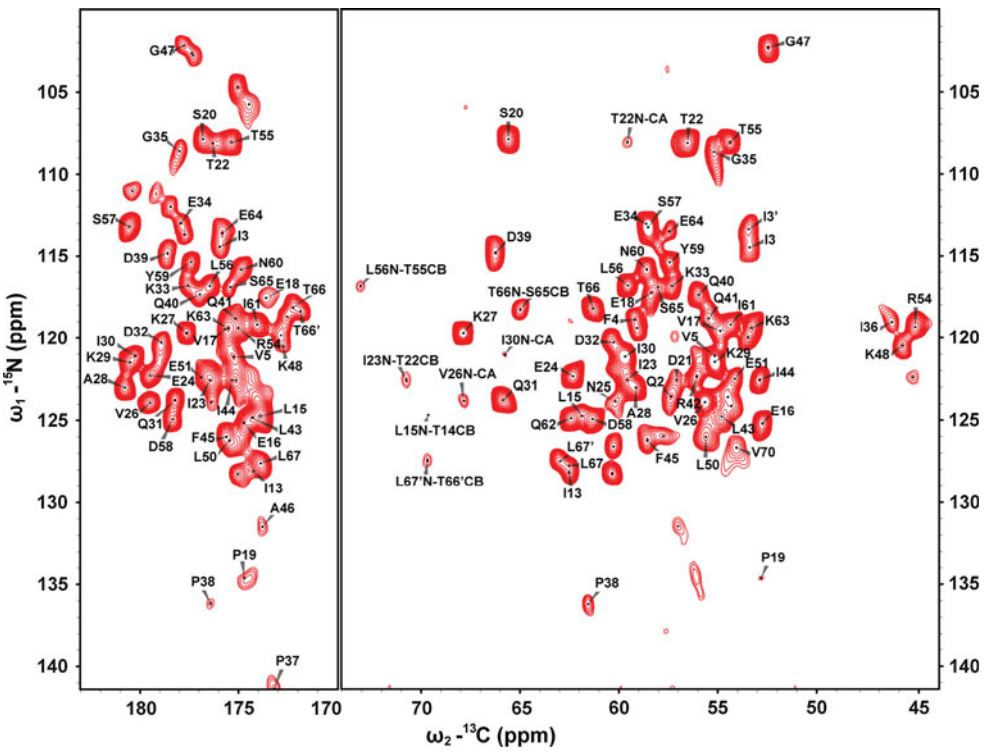

Fig. 5 2D BSH-CP-NCOCA correlation spectrum of uniformly [^{13}C, ^{15}N]-labeled ubiquitin obtained at an MAS frequency of 21 kHz and a magnetic field of 20 T within 12.5 h. Prior to Fourier-transformation, the data were apodized in both dimensions with a 51°-shifted squared sine bell window function. Labels containing *one letter* and *one number* refer to N_iCA_{i-1} and N_iCO_{i-1} correlations. The *prime sign* refers to signals from a second polymorph

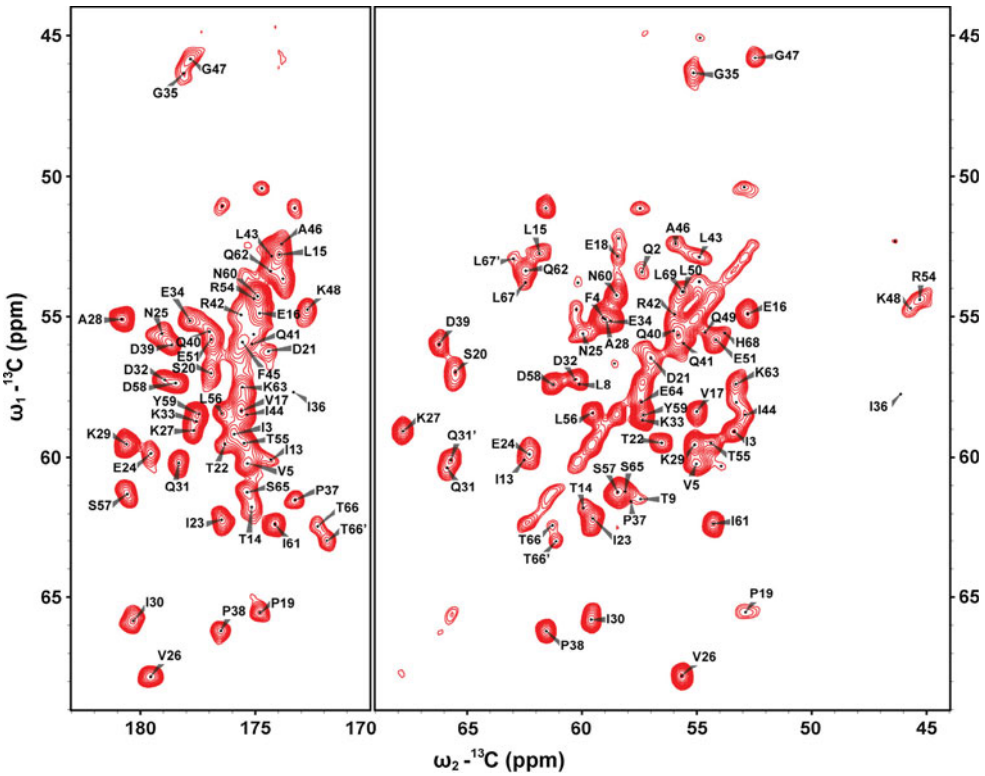

Fig. 6 2D BSH-CP $CA_i(N)COCA_{i-1}$ spectrum of uniformly [^{13}C, ^{15}N]-labeled ubiquitin obtained at an MAS frequency of 21 kHz and a magnetic field of 20 T within 36.5 h. Prior to Fourier-transformation, the data were apodized in both dimensions with a 51°-shifted squared sine bell window function. Labels containing *one letter* and *one number* refer to CA_iCA_{i-1} and CA_iCO_{i-1} correlations. The *prime sign* refers to signals from a second polymorph

discussed effect regarding relay and long-range magnetization PDSD transfer is clearly visible in the overlay. Figure 1 of the Supporting Information shows BSH-CP-NCOCA and NCOCX spectra, both recorded at 21 kHz MAS with BSH-CP and PDSD transfer times of 4 and 50 ms, respectively. Even at the significantly higher spinning rate, long range and/or relay correlations are present in the PDSD-based NCOCX spectrum.

We then recorded a complete set of 2D experiments for backbone assignment based on BSH-CP for efficient CO–CA transfer, in order to demonstrate the high performance of this recoupling technique. BSH-CP-based NCOCA and $CA_i(N)COCA_{i-1}$, as well as NCA and ^{13}C–^{13}C PDSD spectra were recorded within a total time of 72 h. The 2D NCOCA and $CA_i(N)COCA_{i-1}$ spectra exhibit relatively high resolution (limited by the sample quality) and an excellent signal-to-noise ratio, as depicted in Figs. 5, 6, respectively. Figure 2 of the Supporting Information shows the NCA spectrum. We could rapidly identify sequential connectivities, sufficient to assign 66 CA and 56 ^{15}N backbone resonances (See assignment table in the Supporting Information). The assignment of CA is facilitated by the direct CA_i–CA_{i-1} correlations, allowing for the assignment of 10 more CAs than ^{15}N backbone nuclei. Even though for a number of residues the CA assignments of the given and preceding residues are known, the backbone N of the given residue cannot be assigned due to the low N resolution of the 2D BSH-CP-NCOCA and NCA spectra. This clearly demonstrates the usefulness of direct CA_i–CA_{i-1} correlations, which has also been observed before (Siemer et al. 2006; Shi et al. 2009). We observed peak doubling for the residues I3, Q31, S65, T66 and L67, which extends a previous study on a PEG-precipitated sample by Seidel et al. (2005). Similar to previous solid-state NMR investigations on ubiquitin (Igumenova et al. 2004; Seidel et al. 2005) no assignment could be obtained for the last 6 C-terminal residues, which is presumably due to dynamic disorder.

Conclusion

In summary, we have shown that BSH-CP under proton-carbon decoupling is an efficient magnetization transfer method for CO and CA spins in a fully protonated protein, that compares very favorably to PDSD-type experiments which are often applied. The simplicity of the scheme and the high achievable transfer rates of up to 33 % make it strongly appealing for MAS NMR applications to biomolecules. The recoupling method has been employed to obtain interresidual NCOCA and CA_i–CA_{i-1} correlation spectra, allowing for a rapid sequential backbone resonance assignment of PEG-precipitated ubiquitin.

Acknowledgments We thank Karin Giller and Brigitta Angerstein for expert technical assistance. This work was supported by the Max Planck Society, the DFG (Emmy Noether Fellowship to A. L.), and

the European Union Seventh Framework Program under Grant Agreement 261863 (Bio-NMR). C.S. acknowledges funding from the MPG-CAS Joint Doctoral Promotion Programme.

References

Asami S, Rakwalska-Bange M, Carlomagno T, Reif B (2013) Protein-RNA interfaces probed by ^{1}H-detected MAS solid-state NMR spectroscopy. Angew Chem Int Ed 52(8):2345–2349

Baldus M, Petkova AT, Herzfeld J, Griffin RG (1998) Cross polarization in the tilted frame: assignment and spectral simplification in heteronuclear spin systems. Mol Phys 95(6):1197–1207

Bayro MJ, Ramachandran R, Caporini MA, Eddy MT, Griffin RG (2008) Radio frequency-driven recoupling at high magic-angle spinning frequencies: homonuclear recoupling sans heteronuclear decoupling. J Chem Phys 128(5):052321

Bayro MJ, Huber M, Ramachandran R, Davenport TC, Meier BH, Ernst M, Griffin RG (2009) Dipolar truncation in magic-angle spinning NMR recoupling experiments. J Chem Phys 130(11):114506

Bayro MJ, Debelouchina GT, Eddy MT, Birkett NR, MacPhee CE, Rosay M, Maas WE, Dobson CM, Griffin RG (2011) Intermolecular structure determination of amyloid fibrils with magic-angle spinning and dynamic nuclear polarization NMR. J Am Chem Soc 133(35):13967–13974

Bennett AE, Rienstra CM, Griffiths JM, Zhen WG, Lansbury PT, Griffin RG (1998) Homonuclear radio frequency-driven recoupling in rotating solids. J Chem Phys 108(22):9463–9479

Boeckmann A, Gardiennet C, Verel R, Hunkeler A, Loquet A, Pintacuda G, Emsley L, Meier BH, Lesage A (2009) Characterization of different water pools in solid-state NMR protein samples. J Biomol NMR 45(3):319–327

Chevelkov V, Fink U, Reif B (2009) Quantitative analysis of backbone motion in proteins using MAS solid-state NMR spectroscopy. J Biomol NMR 45(1–2):197–206

Chevelkov V, Giller K, Becker S, Lange A (2013) Efficient CO–CA transfer in highly deuterated proteins by band-selective homonuclear cross-polarization. J Magn Reson 230:205–211

De Paepe G (2012) Dipolar recoupling in magic angle spinning solid-state nuclear magnetic resonance. In: Johnson MA, Martinez TJ (eds) Annual review of physical chemistry, vol 63. Annual Reviews, Palo Alto, pp 661–684

Fung BM, Khitrin AK, Ermolaev K (2000) An improved broadband decoupling sequence for liquid crystals and solids. J Magn Reson 142(1):97–101

Hodgkinson P, Emsley L (1999) The accuracy of distance measurements in solid-state NMR. J Magn Reson 139(1):46–59

Hong M, Schmidt-Rohr K (2013) Magic-angle-spinning NMR techniques for measuring long-range distances in biological macromolecules. Acc Chem Res doi: 10.1021/ar300294x

Huang KY, Siemer AB, McDermott AE (2011) Homonuclear mixing sequences for perdeuterated proteins. J Magn Reson 208(1):122–127

Huber M, Hiller S, Schanda P, Ernst M, Bockmann A, Verel R, Meier BH (2011) A proton-detected 4D solid-state NMR experiment for protein structure determination. ChemPhysChem 12(5):915–918

Igumenova TI, Wand AJ, McDermott AE (2004) Assignment of the backbone resonances for microcrystalline ubiquitin. J Am Chem Soc 126(16):5323–5331

Jehle S, Rajagopal P, Bardiaux B, Markovic S, Kuhne R, Stout JR, Higman VA, Klevit RE, van Rossum BJ, Oschkinat H (2010) Solid-state NMR and SAXS studies provide a structural basis for the activation of alpha B-crystallin oligomers. Nat Struct Mol Biol 17(9):1037–1042

Lazar GA, Desjarlais JR, Handel TM (1997) De novo design of the hydrophobic core of ubiquitin. Protein Sci 6(6):1167–1178

Lewandowski JR (2013) Advances in solid-state relaxation methodology for probing site-specific protein dynamics. Acc Chem Res doi: 10.1021/ar300334g

Loquet A, Sgourakis NG, Gupta R, Giller K, Riedel D, Goosmann C, Griesinger C, Kolbe M, Baker D, Becker S, Lange A (2012) Atomic model of the type III secretion system needle. Nature 486(7402):276–279

McDermott A (2009) Structure and dynamics of membrane proteins by magic angle spinning solid-state NMR. Annu Rev Biophys 38:385–403

Mithu VS, Bakthavatsalam S, Madhu PK (2013) ^{13}C-^{13}C homonuclear recoupling in solid-state nuclear magnetic resonance at a moderately high magic-angle-spinning frequency. PLoS ONE 8(1):e50504

Morcombe CR, Gaponenko V, Byrd RA, Zilm KW (2004) Diluting abundant spins by isotope edited radio frequency field assisted diffusion. J Am Chem Soc 126(23):7196–7197

Nielsen NC, Bildsoe H, Jakobsen HJ, Levitt MH (1994) Double-quantum homonuclear rotary resonance: efficient dipolar recovery in magic-angle spinning nuclear magnetic resonance. J Chem Phys 101:1805–1812

Pauli J, Baldus M, van Rossum B, de Groot H, Oschkinat H (2001) Backbone and side-chain ^{13}C and ^{15}N signal assignments of the alpha-spectrin SH3 domain by magic angle spinning solid-state NMR at 17.6 tesla. ChemBioChem 2(4):272–281

Raleigh DP, Levitt MH, Griffin RG (1988) Rotational resonance in solid-state NMR. Chem Phys Lett 146(1–2):71–76

Schanda P, Meier BH, Ernst M (2010) Quantitative analysis of protein backbone dynamics in microcrystalline ubiquitin by solid-state NMR spectroscopy. J Am Chem Soc 132(45):15957–15967

Scholz I, Huber M, Manolikas T, Meier BH, Ernst M (2008) MIRROR recoupling and its application to spin diffusion under fast magic-angle spinning. Chem Phys Lett 460(1–3):278–283

Schuetz A, Wasmer C, Habenstein B, Verel R, Greenwald J, Riek R, Bockmann A, Meier BH (2010) Protocols for the sequential solid-state NMR spectroscopic assignment of a uniformly labeled 25 kDa protein: HET-s(1-227). ChemBioChem 11(11):1543–1551

Seidel K, Lange A, Becker S, Hughes CE, Heise H, Baldus M (2004) Protein solid-state NMR resonance assignments from (^{13}C, ^{13}C) correlation spectroscopy. Phys Chem Chem Phys 6(22): 5090–5093

Seidel K, Etzkorn M, Heise H, Becker S, Baldus M (2005) High-resolution solid-state NMR studies on uniformly [^{13}C, ^{15}N]-labeled ubiquitin. ChemBioChem 6(9):1638–1647

Sengupta I, Nadaud PS, Helmus JJ, Schwieters CD, Jaroniec CP (2012) Protein fold determined by paramagnetic magic-angle spinning solid-state NMR spectroscopy. Nat Chem 4(5):410–417

Shaka AJ, Keeler J, Frenkiel T, Freeman R (1983) An improved sequence for broad-band decoupling—WALTZ-16. J Magn Reson 52(2):335–338

Shi LC, Ahmed MAM, Zhang WR, Whited G, Brown LS, Ladizhansky V (2009) Three-dimensional solid-state NMR study of a seven-helical integral membrane proton pump-structural insights. J Mol Biol 386(4):1078–1093

Siemer AB, Ritter C, Steinmetz MO, Ernst M, Riek R, Meier BH (2006) ^{13}C, ^{15}N resonance assignment of parts of the HET-s prion protein in its amyloid form. J Biomol NMR 34(2):75–87

Szeverenyi NM, Sullivan MJ, Maciel GE (1982) Observation of spin exchange by two-dimensional fourier-transform ^{13}C cross polarization-magic-angle spinning. J Magn Reson 47(3):462–475

Takegoshi K, Nomura K, Terao T (1995) Rotational resonance in the tilted rotating–frame. Chem Phys Lett 232(5–6):424–428

Takegoshi K, Nakamura S, Terao T (2001) ^{13}C-^{1}H dipolar-assisted rotational resonance in magic-angle spinning NMR. Chem Phys Lett 344(5–6):631–637

Verel R, Ernst M, Meier BH (2001) Adiabatic dipolar recoupling in solid-state NMR: the DREAM scheme. J Magn Reson 150(1): 81–99

Wasmer C, Lange A, Van Melckebeke H, Siemer AB, Riek R, Meier BH (2008) Amyloid fibrils of the HET-s(218–289) prion form a beta solenoid with a triangular hydrophobic core. Science 319(5869):1523–1526

Weingarth M, Baldus M (2013) Solid-State NMR-Based Approaches for Supramolecular Structure Elucidation. Acc Chem Res doi: 10.1021/ar300316e